ELSEVIER

International Journal of Pharmaceutics 199 (2000) 7–16

international journal of pharmaceutics

www.elsevier.com/locate/ijpharm

Mapping PET-measured triamcinolone acetonide (TAA) aerosol distribution into deposition by airway generation

Zhenghong Lee [a,*], Marc S. Berridge [a,b], Warren H. Finlay [c], Donald L. Heald [d]

[a] *Nuclear Medicine, Radiology, University Hospitals of Cleveland, Cleveland, OH 44106, USA*
[b] *Radiology, School of Medicine, Case Western Reserve University, Cleveland, OH 44106, USA*
[c] *Mechanical Engineering, University of Alberta, Edmonton, Alta., Canada T6G 2G8*
[d] *Clin. Pharm. and Pharmacokinetics, Rhone-Poulenc Rorer Pharm., Collegeville, PA 19426, USA*

Received 11 August 1999; received in revised form 8 December 1999; accepted 5 January 2000

Abstract

The three dimensional (3D) distribution of inhaled drugs was measured using Positron Emission Tomography (PET) (Berridge, M.S, Muswick, G.J., Lee, Z., Leisure, G.L., Nelson, A.D., Muzic, R.F. Jr., Miraldi, F., Heald, D.L., 1997. PET evaluation of Azmacort® ([C-11]triamcinolone acetonide) dose administration. J. Nucl. Med. 38 (5) Suppl., 4–5). Data analysis was based upon regional ratios or penetration indices. To improve the analytical usefulness and objectivity, labeled drug from dynamic PET images was mapped into 23 airway generations following a general framework from a SPECT-based methodology (Fleming, J.S., Nassim, M.A., Hashish, A.H., Bailey, A.G., Conway, J., Holgate, S., Halson, P., Moore, E., Martonen, T.B., 1995. Description of pulmonary deposition of radiolabeled aerosol by airway generation using a conceptual three dimensional model of lung morphology. J. Aerosol Med. 8, 341–356). A recently developed airway network model was used in this study. Quantitative PET scans of [C-11]triamcinolone acetonide distribution in the lung were determined following administration of Azmacort®, a commercial metered dose inhaler with an integrated spacer device. Distributions at varying time periods after drug administration were investigated to explore the dynamics and kinetics of the aerosolized drug. Initially, deposition of labeled drug on conducting airways (generations 1–14) was found to be higher than those on acinar airways (generation 15–23), 64% versus 36%. The distribution pattern changed slowly with time. By 47 min, 51% of the dose remaining in the lung was found on conducting airways while 49% was on acinar airways. This study illustrates the value of PET imaging for the evaluation and design of drug formulations.

Keywords: Aerosol; Inhalation mapping; Three-dimensional measurement; Pulmonary deposition; Dynamic analysis

* Corresponding author.

0378-5173/00/$ - see front matter
PII: S0378-5173(00)00342-2

1. Introduction

1.1. Overview

Evaluation of 3D deposition pattern from aerosol inhalation by means of imaging is important in the optimization and standardization of targeted delivery and aerosol therapy. Planar gamma scintigraphy has limited ability to provide this information due to the two dimensional (2D) nature of the images (Phipps et al., 1989; Martonen et al., 1995a). The application of 3D imaging modalities such as Single Photon Emission Computed Tomography (SPECT) or Positron Emission Tomography (PET) permits proper assessment of the spatial distribution of inhaled drug thus overcoming the principle limitations of planar imaging (Perring et al., 1994; Martonen et al., 1995b). Currently, the quantitative criterion for assessing aerosol lung deposition is the penetration index, which is the ratio of peripheral zone to central zone deposition. This index is computed from planar data based on boxed regions defined according to Agnew et al. (1984). When the 3D biodistribution is known, however, the index may be advantageously replaced by more natural and detailed information such as the deposition in airway generations. Utilizing such a description of aerosol distribution helps to provide valuable information on the distribution of drug in airway tree morphology. This paper describes improvements upon a previous work done in mapping airway generational deposition of inhaled aerosols.

1.2. Limitations of the previous mapping methodology

Pioneering work by Fleming et al. mapped SPECT-measured aerosolized Tc-99m labeled particle distribution into a deposition pattern in relation to airway generations (Fleming et al., 1995; Hashish et al., 1998). The spatial distribution of drug in the lung measured by SPECT and thoracic anatomy from Computer Assisted Tomography (CT) scans were transformed and matched with a conceptual model of the airway network. The model was deduced by scaling and morphing a typical data set of airway dimensions to fit an individual's lung morphology. However, there are several shortcomings associated with this SPECT-based mapping procedure. In particular, Tc-99m labeling serves as a surrogate marker for the drug and thus could yield absorption rates different than those of the drug. It is known that the absorption rate of Tc-99m is not related to drug absorption and, in the case of pertechnetate, is rapid (Perring et al., 1994). Besides, the scanning time required by SPECT is relatively long (≈ 15 min) so that temporal changes of the tracer activity distribution during this imaging period are averaged. As a consequence, it is difficult to estimate the initial aerosol deposition using SPECT. In addition, attenuation and scatter corrections remain as challenges for accurate quantification by SPECT (Tsui, 1995). Finally, the airway dimensions used to derive the conceptual 3D model of lung morphology in Fleming et al.'s work were based on Weibel's data (Weibel, 1963, 1991). Although popular and convenient for analytical work, Weibel's model is highly idealized due to extrapolation and smooth interpolation of the measured data from a partial cast of a human lung.

1.3. Improvement implemented in this study

Data from PET scans generated on materials with identical particle size distribution for the tracer and aerosolized drug were used in this study. Operating in the dynamic mode, PET scans minimize the temporal averaging problem that occurs during the longer SPECT scans. In addition, scatter and attenuation corrections are relatively straightforward to implement for PET (Ollinger and Fessler, 1997). Also, a more realistic lung model was used for airway dimensions. It was obtained from a statistical reconstruction of airways based on measured data from a more complete human cast (Phillips et al., 1994a).

2. Material and methods

2.1. PET and CT scans

Lung distribution of [C-11]triamcinolone acetonide (TAA) formulated as Azmacort® (Rhone-

Poulenc Rorer Pharmaceuticals, RPR, Collegeville, PA, USA) in a metered dose inhaler was scanned using a Siemens ECAT EXACT 921 PET camera (Siemens/CTI PET Systems, Knoxville, TN, USA). Transmission and emission images were acquired using three bed positions for a contiguous volume set covering the head and thorax of each volunteer. Normal healthy male volunteers with the following inclusion criteria were used in the study: age between 18 and 50 years, weight within $\pm 15\%$ of the reported mean values for their height as determined by Metropolitan Life Tables, $FEV_1 \geq 80\%$ of predicted, non-smoker, no concomitant medications. Volunteers also met the following exclusion criteria: no history of significant cardiovascular, neurological, hepatic, renal, or respiratory medical conditions; no clinically relevant deviation from normal in physical or laboratory tests (Chem 23, CBC, w/diff, urine analysis); and no history of hypersensitivity to corticosteroids. Four normal volunteers ($n = 4$) meeting the inclusion and exclusion criteria were selected for the study, the protocol being previously approved by IRB. The positron-emitting C-11 was incorporated into the drug molecule via isotopic substitution (Berridge et al., 1997). The labeled formulation met the supplier's criteria for particle size distribution, dose delivery, content uniformity, and canister performance. Drug administration to the volunteers was performed immediately after preparation was finished. Upon completion of the scans, cascade impactor determinations were performed on each canister used. The dose dispensed from the canister was also measured in units of both mass and radioactivity to ensure stability of the product during the study. Like the initial assays, all post-dose stability studies met the supplier's acceptance criteria. Dynamic PET emission data were corrected for scatter by a de-convolution procedure (Lercher and Wienhard, 1994) and for attenuation from a measured attenuation map (Kouris, 1984; Buvat et al., 1996). Emission data were also decay corrected.

CT scans were taken on the same day as the PET scan using a Siemens Somatom 4 + B spiral CT system with power package (Siemens Medical System, Iselin, New Jersey, USA). CT acquisition from head to abdomen was divided into two segments; one with breath holding for the thorax region, and the other without breath holding for the head (mouth and throat). Using fiducial markers and anatomic landmarks, CT and dynamic PET images were aligned. The boundary of the lung region was delineated from the CT data. The edge detection technique, region-growing, was used (Gonzalez and Wintz, 1987) in a semi-automatic mode. CT data were used to calculate tissue density (Fleming, 1989). Alternatively, PET transmission data were also used for the same density estimation.

2.2. A new model for lung morphometry

Various models describing the variations of airway dimensions from the trachea to the periphery have been developed by lung morphologists and mathematicians. These models are structured in a hierarchical fashion to follow the branching pattern observed from human lung casts. Two approaches are generally used to construct the models: (1) generation downward, starting at the trachea and going downward along the tree (Weibel, 1963); (2) converging orders upwards, beginning at the periphery and coming back to the center like a confluent river system (Horsfield et al., 1971). In Weibel's updated model, airways were ordered from 0 (trachea) to 23 (alveolar sac) generations, in which generations 0–14 represented the conducting airways and generations 15–23 were named the acinar airways (Weibel, 1991). However, Weibel's model has limitations. It assumes a symmetrical tree branching pattern with strict dichotomy and uses a partial resin cast of the human lung to deduce dimensions for the intermediate or transitional airway (generations 11–15). As a consequence, the derived data set loses some characteristic features of the airway network (Phillips et al., 1994a).

Recently, a statistical reconstruction technique to restore the missing airways has been made (Phillips et al., 1994a,b). This airway diameter-oriented analysis was carried out on measurements made by Raabe et al. (1976) and represent the most detailed published morphometric data available on the human bronchial tree. Regrettably, this more complete morphometric model is not in a form

suitable for mapping aerosol deposition in the present investigation. A new generation-ordered lung model (Finlay et al., 1999) that combines data on the tracheo-bronchial region (Phillips et al., 1994a; Phillips and Kaye, 1995) with aveolar data from other investigators (Haefeli-Bleuer and Weibel, 1988) is now available that makes it possible to develop an asysmmetrical model of the conducting airways which upon averaging across the respective branches for each generation yields a more comprehensive symmetrical model for lung deposition studies. Like all the other generation-ordered lung morphometrics, airway dimensions of the new model were thus calculated to characterize the mean value for each generation. Dimensional data include number, length, diameter, and volume of each airway generation and are available in the literature (Weibel, 1963, 1991; Finlay et al., 1999).

2.3. The mapping procedure

The reason for performing the mapping is twofold. First, the measured deposition of inhaled [C-11]-labeled TAA in the thorax from the PET emission scan provided a 3D distribution of drug in the lung which is not the desired description of targeted deposition. The mapping procedure described in this section converts the measured spatial distribution into a generational deposition pattern. Secondly, the resolution of the state-of-art medical imaging scanners is not fine enough both for depicting the geometry of smaller airway (CT) and for directly describing the acinar deposition quantity (PET). However, using a conceptual model as a bridge, the crude regional distribution is re-assigned (mapped) through a mathematical operation to airway generational deposition. Airway dimensions derived from a FRC (functional residual capacity of the lung) varies from subject to subject, thus requiring that the standard data set be scaled to fit an individual's lung capacity. In the present investigation, linear dimensions such as diameter and length were scaled to the cube root of volume. The mapping procedure used in this study is briefly summarized here. It followed the general framework of Fleming et al.'s mapping method (Fleming et al., 1995, 1996), but with the following distinctions:

1. Dynamic PET scans of the distribution of labeled TAA were used instead of SPECT scans of Tc-99m that had been added to the drug formulation;
2. Finlay et al.'s lung model was used in place of Weibel's model;
3. The lungs were not assumed to be of equal size when scaling the mean total air volume to match the cumulative volume in the model;
4. Different concentration patterns for acinar airways were explored.

The measured data within the lung, including the activity distribution from PET and the anatomic morphology from CT, were transformed into concentric hemispherical shells according to their relative radial distance from the carina. These hemispherical shells represented the first-order approximation of the lung. They provided a standardized intermediate representation for fitting the detailed airway model into individual anatomic data. Ten such shells were obtained with approximately 10 mm thickness each. The system resolution of PET imaging is approximately 7 mm. However, tidal breathing during the PET scans had a blurring effect on the images. The overall resolution is close to 9–10 mm, similar to the size of each shell. The total activity (s_i) of each shell i was obtained by summing all the activities in shell i. If one assumes that aerosol is distributed according to air volume and that deposition efficiency within each airway generation is uniform, the deposition will be proportional to the air volume in each shell and the following equation will hold:

$$s_i = \sum_{j=1}^{23} V_{ij} \cdot g_j / G_j \quad (1)$$

where s_i is the activity of each shell i as mentioned above, and G_j is the air volume of airway generation j which can be derived from the lung model. The most important parameter is matrix V_{ij}, the volume of each airway generation j present in each shell i. This is the heart of the conceptual model. V_{ij} was computed based on measured lung size and density distribution from CT, and on airway dimensions of Finlay et al.'s lung model scaled for individual lung volume. The procedure for computing the matrix V_{ij} was fully described

in Fleming et al.'s work (1995). His algorithm solved Eq. (1) for the only remaining unknown, g_j, which is the desired deposition in each airway generation j. Further assumptions about the deposition pattern were needed for the algorithm. Details of the algorithm along with its assumptions were described in the original work (Fleming et al., 1995). Among the total 24 generations of airways in the model lung, generation 0 (the trachea) is not included in Eq. (1) since the trachea is completely outside the lung and excluded when analyzing the PET lung images. The mapping algorithm consists of two parts. One of them is for the conducting airway using the conceptual lung model. The other is for the acinar airways. For conducting airways, we adopted the same assumptions as Fleming et al. For acinar airways, the situation is delicate. Fleming et al. assumed: (1) concentrations of aerosol were equal in the generations at the transition between conducting and acinar airways; (2) concentrations of aerosol decreased linearly with generation number for the acinar airways but were subject to the constraint of the known total activity in the acini. The formula bearing these two assumptions is

$$c_j = c_{14} - m \cdot (j - 15) \quad j = 15, 16, \ldots 23 \tag{2}$$

where c_j is the concentration or activity per unit air volume in generation j and m is a constant. An acinar airway activity concentration, which decreased with airway generation, was conceivable, but a steady and linear decrease may lead to negative values for the concentrations in higher airway generations. The constraint guaranteed mass conservation but did not prevent negativity. We therefore proposed speculatively that the concentration might follow an exponentially decreasing pattern as Eq. (3).

$$c_j = c_{j-1} \cdot \alpha^{k+j-15} \quad j = 15, 16, \ldots 23 \tag{3}$$

where the base α was tested for values between 1.0 and 2.0 and the rate of decrease k, in the exponential was determined according to the constraints of Fleming et al. Equal concentrations between generations 14 and 15 were not assumed in this model.

3. Results

3.1. Hemisphere

The radius of the hemispheres after the hemispherical transform averaged 9.05 cm. Divided into ten equal concentric shells along the radius, the averaged thickness of each shell was 9.05 mm. The estimation of tissue densities in the lung region along with other parameters was calculated from a CT scan, shown in Table 1. CT data gave the density of the middle to outer lung shells a value ≈ 0.30 g/ml, similar to the known values in the literature and thus considered correct (Metry et al., 1997).

In Fleming et al.'s work, the left and right lungs were assumed to be equal in size during the scaling. However, due to the position of the heart, the left lung is always smaller than the right lung. In this study, an estimation of the air volume from the left lung was also computed along with that from the right lung. Standard airway dimensions were thus scaled for each individual without the assumption of equally sized lungs.

Table 1
Parameters of shell structures from the hemispherically transformed lung

Shell number	1	2	3	4	5	6	7	8	9	10
Shell volume (cm^3)	1.34	10.36	37.37	71.16	120.5	193.8	263.1	355.3	468.2	737.6
Density* (g/cm^3)	0.95	0.79	0.51	0.40	0.33	0.29	0.27	0.26	0.27	0.52**
Air volume (cm^3)	0.30	2.16	18.12	42.15	80.10	136.5	190.9	262.2	345.5	544.3

* Density calculation is based on converting CT numbers.

** The large value for the out-most shell is due to partial volume averaging at the lung boundary and was not used. The value from shell $\#9$ was used for shell $\#10$.

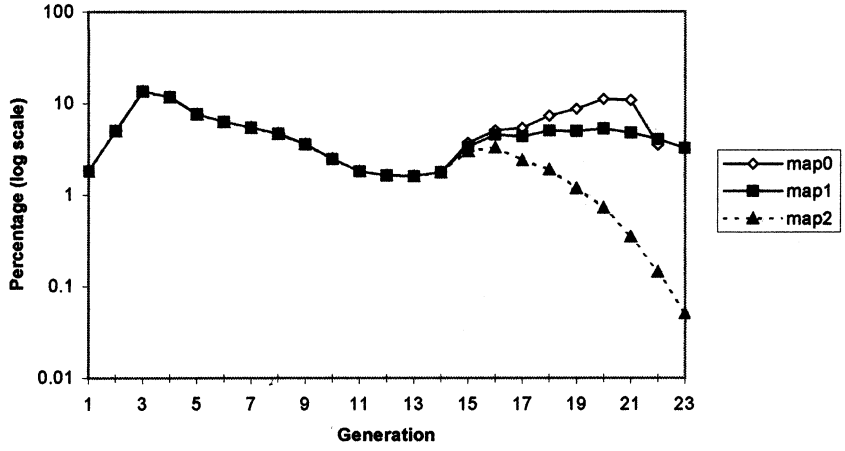

Fig. 1. Acinar airway pattern on logarithmic scale: map0 is the linear pattern; map1 and map2 are the exponential patterns with $\alpha = 1.1$ and 1.2, respectively, see text.

3.2. Acinar concentration

The acinar airway mapping depended heavily on the assumption about the activity concentration pattern. If we assumed a linear decrease of activity concentration along the acinar airway generations, the concentration decreased according to Eq. (2) but reached negative values in the distal generations in most cases. For the exponentially decreasing model of Eq. (3), the results of using different decreasing patterns for mapping are shown semi-logarithmically in Fig. 1. The data chosen were an initial drug deposition from one of the Azmacort® inhalations. For the conducting airways, generations 1–14, the mapping is unique. For the acinar portion, three mappings are shown: 'map0', the linear decreasing model; 'map1', the exponential model $\alpha = 1.1$; and 'map2' $\alpha = 1.2$. The last data point of 'map0' could not be shown because of its negative value. For the case of 'map2', $\alpha = 1.2$ appears to be too large since the deposition pattern rapidly approached zero. In addition, mass conservation no longer held for this pattern. Only 'map1' with $\alpha = 1.1$ seemed acceptable and was chosen for the acinar airway mapping. For all values of α tested, the acinar distribution followed the pattern of initially increasing and then decreasing towards the distal generations.

3.3. Overall pattern and its dynamics

Smoothly varying bimodal distributions were observed for all inhalations of C-11 labeled Azmacort® studied. Fig. 2 shows the initial deposition from different volunteers on a linear scale. The percentages were normalized to the total dose in the lung. The distribution reached a maximum in the first few generations and slowly declined to a minimum between generations 12–13. The curves reached a second lower peak in the acini before descending towards zero at the periphery. Distribution patterns were similar for all volunteers studied although variations among them were observed. The normalized data were grouped into conducting and acinar depositions by summing up depositions on airways from generations 1–14, and from 15–23, respectively. The results are shown in Table 2. The initial depositions on conducting airways were higher and accounting for 60–68% of the drug dose in the lung, with the remainder on the acinar airways. The results were consistent with the visual impression given by the PET images.

Dynamic PET data are mapped for each volunteer and summarized in Table 2. One of the mappings is shown in Fig. 3. Percentages in the figure were decay-corrected and scaled according to the initial deposition. The general bimodal

distribution pattern remained at all times. The 5-min data (scan # 2) closely resembled the initial deposition for all volunteers. After 47 min (scan # 5), the distribution patterns were noticeably different from the initial data. The overall drug in the lung decreased to about 44% of the initial dose due to the clearance and/or absorption in the lung. The minimum in the distribution curve moved from generation 13 to 10 at 47 min. In general, the remaining deposition in conducting airways fell more quickly than that in acinar airways. At 47 min, only 51% of the drug left in the lung was found on the conducting airways while 49% was on the acinar airways. The changes of relative percentage depositions, after 47 min, between conducting and acinar airways were significant compared to the initial depositions ($F_s =$ 10.125 when $F_{0.05}[1, 12] = 4.747$ from two-way ANOVA).

4. Discussions

4.1. Scans and model

There are four advantages to using PET over gamma scintigraphy (2D) or SPECT for 3D lung aerosol deposition measurement. The drug is isotopically labeled so there is no chance for a violation of tracer principle, as may happen with other labeling approaches. Dynamic PET scans allow regional kinetics of the drug to be observed and do not undergo the kinetic averaging produced by long scanning time. The spatial and

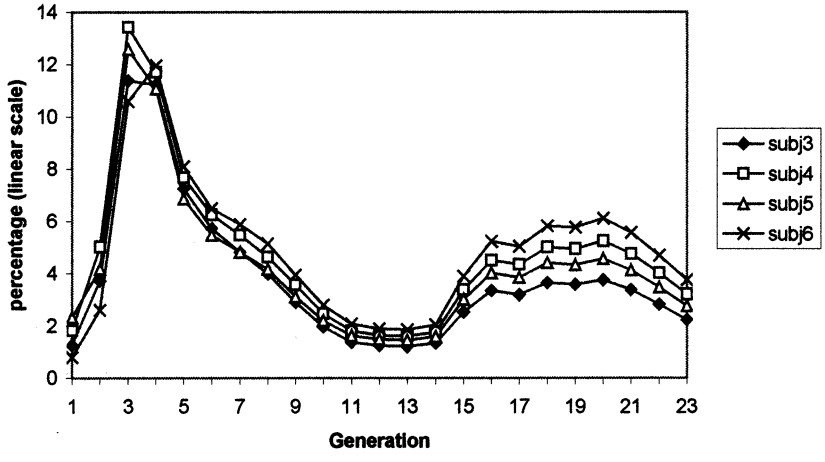

Fig. 2. Initial airway depositions, resulted from the mapping and on linear scale, of all subjects after inhalation of Azmacort®.

Table 2
Normalized percentage dose (%) mapped from volunteers after inhalations of Azmacort®

	Conducting airways*			Acinar airways*		
Time**	0	5	47	0	5	47
Subject # 3	67.57	68.26	69.05	32.43	31.74	30.95
Subject # 4	63.57	64.37	48.89	36.43	35.63	51.11
Subject # 5	64.52	64.79	38.88	35.48	35.21	61.11
Subject # 6	59.04	60.33	47.94	40.96	39.67	52.06

* The total dose was divided into two percentage depositions: conducting, from generations 1–14; acinar, from 15–23.
** Time indicates the instant from the beginning of PET scan, in min.

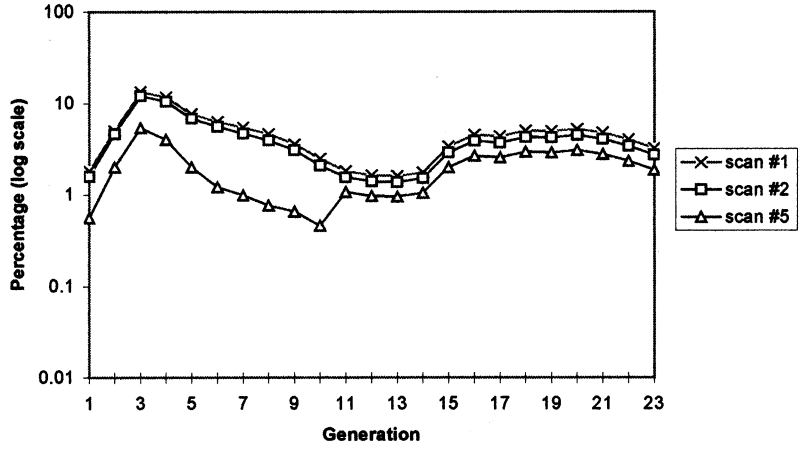

Fig. 3. Changing airway depositions with time mapped from one volunteer after Azmacort® inhalation: scan #1 is the initial deposition; scans #2 and #5 are the depositions after 5 and 47 min from the initial. Similar dynamic mappings were obtained from other volunteers, but not shown for the clarity of the figure.

temporal resolutions of PET are higher than those of SPECT. Corrections for tissue attenuation and γ photon scattering can be implemented reliably in PET. Both corrections are vital for quantification of deposition of aerosol particles.

The need for a model to estimate the generational distribution of drug deposition arises because it is not currently possible to image drug deposition at the resolution of the smallest airways. The algorithm that relates generational deposition to the observed distribution in the lung is quite complex and lung size is variable. This required that the intermediate hemispherical shell model of the lung be used as a standardized platform for the airway mapping procedure.

4.2. Acinar assumptions

The calculation of deposition on the conducting airways (generations 1–14) was unique and apparently reliable. Although the total activity in the acini was known, the calculated deposition pattern was not unique. The linear decreasing model was intuitive, and once assumed, the decreasing slope could be determined uniquely. However, with the linear model, negative concentration results were obtained. To overcome this negativity, we proposed an exponentially decreasing model for the drug concentration in the acinar airway. Whether the two parameters obtained for the exponential model were optimal remains to be seen.

Drug distribution in the acinar airways appeared to depend on the conducting airways, parameters of the exponential model, airway dimensions from the lung model, and finally on the measured data. Although the airway was scaled to match each FRC, the proportions among the dimensions from the lung model were preserved. These facts explain, in part, why the deposition patterns of the acinar airway did not change appreciably between individuals or as a function of time in contrast to deposition in the conducting airways. Future work will need to focus on acinar airway deposition mapping. More emphasis needs to be given to the measured data and less to the model parameters to help further differentiate the deposition patterns among individuals for that portion of the airway tree.

4.3. Conclusion

This technique of analyzing in vivo drug distribution is a powerful tool. The target-oriented deposition analysis provides a more detailed interpretation of pulmonary distribution of particles

than spatial regional analysis, e.g. the penetration index analysis. The dynamic sequence of PET scans allowed examination of the evolution of deposition along airway generations with time. The conducting airways showed more manifest changes with time than the acinar airways. This is likely due to the normal clearance mechanisms (Guyton, 1991). We expect these techniques to be useful for evaluation and design of drug formulations using PET.

Acknowledgements

The authors thank anonymous referees for their editorial effort to improve the article. We thank Dr Fleming for sharing the details of his mapping procedure and for helpful comments. We also thank the CWRU Clinical Research Center (CRC) for technical assistance with the human subject portion of this work. The CRC is supported in part by NIH (NCRR MO1RR00080). This project was supported in part by Rhone-Poulenc Rorer Pharmaceuticals.

References

Agnew, J.E., Bateman, R.M., Pavia, D., Clark, S.W., 1984. Radionuclide demonstration of ventilatory abnormalities in mild asthma. Clin. Sci. 66, 525–531.

Berridge, M.S, Muswick, G.J., Lee, Z., Leisure, G.L., Nelson, A.D., Muzic, R.F. Jr., Miraldi, F., Heald, D.L., 1997. PET evaluation of Azmacort® ([C-11]triamcinolone acetonide) dose administration. J. Nucl. Med. 38 (5) Suppl., 4–5.

Buvat, I., Freedman, N.M.T., Dilsizian, V., Bacharach, S.L., 1996. Realignment of emission contaminated attenuation maps with uncontaminated attenuation maps for attenuation correction in PET. J. Comput. Assist. Tomogr. 20, 848–854.

Finlay, W.H., Lange, C.F., Li, W.-I., Hoskinson, M., 1999. Validating deposition models in disease: what is needed? J. Aerosol Med. (in press).

Fleming, J.S., 1989. A technique for using CT images in attenuation correction and quantification in SPECT. Nucl. Med. Comm. 10, 83–97.

Fleming, J.S., Nassim, M.A., Hashish, A.H., Bailey, A.G., Conway, J., Holgate, S., et al., 1995. Description of pulmonary deposition of radiolabeled aerosol by airway generation using a conceptual three dimensional model of lung morphology. J. Aerosol Med. 8, 341–356.

Fleming, J.S., Halson, P., Conway, J., Moore, E., Nassim, M.A., Hashish, A.H., et al., 1996. Three-dimensional description of pulmonary deposition of inhaled aerosol using data from multimodality imaging. J. Nucl. Med. 37, 873–877.

Gonzalez, R.C., Wintz, P., 1987. Digital Image Processing, second edn. Addison-Wesley, Readings, MA, pp. 368–375.

Guyton, A., 1991. Pulmonary ventilation. In: Textbook of Medical Physiology, eight edn. W.B. Saunders Company, Philadelphia, p. 402.

Haefeli-Bleuer, B., Weibel, E.R., 1988. Morphometry of the human pulmonary acinus. The Anatom. Record 220, 401–414.

Hashish, A.H., Fleming, J.S., Conway, J., Halson, P., Moore, E., Williams, T.J., et al., 1998. Lung deposition of particles by airway generation in healthy subjects: three-dimensional radionuclide imaging and numerical model prediction. J. Aerosol Sci. 29, 205–215.

Horsfield, K., Dart, G., Olson, D.E., Filley, G.F., Cumming, G., 1971. Models of the human bronchial tree. J. Appl. Physiol. 31, 207–217.

Kouris, K., 1984. Emission tomography: a concise theoretical overview. Nucl. Med. Commun. 5, 733–739.

Lercher, M.J., Wienhard, K., 1994. Scatter correction in 3D PET. IEEE Trans. Med. Imag. 13, 649–657.

Martonen, T.B., Yang, Y., Hwang, D., Fleming, J.S., 1995a. Computer simulations of human lung structures for medical applications. Comput. Biol. Med. 25, 431–446.

Martonen, T.B., Yang, Y., Hwang, D., Fleming, J.S., 1995b. Computer model of human lung morphology to complement SPECT analysis. Int. J. Bio-Med. Comput. 40, 5–16.

Metry, G., Wegenius, G., Wikstrom, B., Kallskog, V., Hansell, P., Lindgren, P.G., et al., 1997. Lung density for assessment of hydration status in hemodialysis patients using the computed tomographic densitometry technique. Kidney Int. 52, 1635–1644.

Ollinger, J.M., Fessler, J.A., 1997. Positron-emission tomography. IEEE Signal Proc. Mag. 14, 43–55.

Perring, S., Summers, Q., Fleming, J.S., Nassim, M.A., Holgate, S.T., 1994. A new method of quantification of the pulmonary regional distribution of aerosols using combined CT and SPECT and its application to nedocromil sodium administered by metered dose inhaler. Br. J. Radiol. 67, 46–53.

Phillips, C.G., Kaye, S.R., 1995. Diameter-based analysis of the branching geometry of four mammalian bronchial trees. Respir. Physiol. 102, 303–316.

Phillips, C.G., Kaye, S.R., Schroter, R.C., 1994a. A diameter-based reconstruction of the branching pattern of the human bronchial tree, Part I. Description and application. Respir. Physiol. 98, 193–217.

Phillips, C.G., Kaye, S.R., Schroter, R.C., 1994b. A diameter-based reconstruction of the branching pattern of the human bronchial tree, Part II. Mathematical formulation. Respir. Physiol. 98, 219–226.

Phipps, P.R., Gonda, I., Bailey, D.L., Borham, P., Bautovich, G., Anderson, S.D., 1989. Comparisons of planar and tomographic gamma scintigraphy to measure the penetration index of inhaled aerosols. Am. Rev. Respir. Dis. 139, 1516–1523.

Raabe, O.G., Yeh, H.C., Schum, G.M., Phalen, R.F., 1976. Tracheobronchial Geometry: Human, Dog, Rat, Hamster. LF-53. Lovelace Foundation for Medical Education and Research, Albuquerque, NM.

Tsui, B.M.W., 1995. SPECT (single-photon emission computed tomography). In: Bronzino, J.D. (Ed.), The Biomedical Engineering Handbook. CRC Press: IEEE Press, Boca Raton, pp. 1055–1073.

Weibel, E.R., 1963. Morphometry of the Human Lung. Academic Press, New York, pp. 136–143.

Weibel, E.R., 1991. Design of airways and blood vessels considered as branching tree. In: Crystal, R.G., et al. (Eds.), The Lung: Scientific Foundations. Raven Press, New York, pp. 711–720.